



This is a repository copy of *Behaviour of composite slab-beam systems at elevated temperatures: Experimental and numerical investigation.*

White Rose Research Online URL for this paper:
<http://eprints.whiterose.ac.uk/87190/>

Version: Accepted Version

Article:

Nguyen, T-T., Tan, K-H. and Burgess, I.W. (2015) Behaviour of composite slab-beam systems at elevated temperatures: Experimental and numerical investigation. *Engineering Structures*, 82. 199 - 213. ISSN 0141-0296

<https://doi.org/10.1016/j.engstruct.2014.10.044>

Reuse

Unless indicated otherwise, fulltext items are protected by copyright with all rights reserved. The copyright exception in section 29 of the Copyright, Designs and Patents Act 1988 allows the making of a single copy solely for the purpose of non-commercial research or private study within the limits of fair dealing. The publisher or other rights-holder may allow further reproduction and re-use of this version - refer to the White Rose Research Online record for this item. Where records identify the publisher as the copyright holder, users can verify any specific terms of use on the publisher's website.

Takedown

If you consider content in White Rose Research Online to be in breach of UK law, please notify us by emailing eprints@whiterose.ac.uk including the URL of the record and the reason for the withdrawal request.



eprints@whiterose.ac.uk
<https://eprints.whiterose.ac.uk/>

Behaviour of Composite Slab-Beam Systems at Elevated Temperatures: Experimental and Numerical Investigation

T.-T. Nguyen¹, K.-H. Tan²

School of Civil and Environmental Engineering, Nanyang Technological Univ., Singapore

I. W. Burgess³

Department of Civil and Structural Engineering, University of Sheffield, United Kingdom

Abstract

This paper presents the experimental observations and results of three one-quarter scale composite slab-beam systems, 3.15m by 3.15m in plan, and tested in fire conditions. The tests aimed to examine the effects of unprotected interior secondary beams and edge rotational restraint on the behaviour of floor assemblies. The test results show that continuity of reinforcement in the slab over the supporting beams, and the presence of interior beams, can reduce the slab deflection and enhance its load-bearing capacity. Interior beams can be left unprotected without leading to a structural failure. The interior beams play a major role in helping the slab to move from biaxial bending stage to membrane behaviour, enabling the slab to mobilize higher tensile membrane forces. Rotational restraint along the protected edge beams induces intense stress concentration above these beams, resulting in more severe concrete crushing at the four corners and wide cracks over the edge beams. The test results are compared to the Bailey-BRE method adopted in SCI publication P288. The method gives conservative results for the case with unprotected interior beams. However, it is recommended that it should not be applied for slab panels without interior beams because the failure mode for these was in a “brittle” mode which would occur suddenly. In addition to the experimental study, a numerical model using ABAQUS has been developed to simulate the tests. The numerical predictions agree well with the experimental results, showing that the proposed model is reliable.

Keywords: Tensile membrane action, Slab-beam systems, Restraint, Composite slabs, Fire.

¹ PhD Candidate (corresponding author), nguyentt@ntu.edu.sg; Tel: +65 67905077

² Professor of Structural Engineering

³ Professor of Structural Engineering

1 Introduction

Large-scale fire tests, as well as well-publicised accidental building fires over the past two decades, have shown that under fire conditions composite-steel-framed floor systems possess a significant load-bearing capacity, which can be well above that predicted by conventional yield line theory. It is now accepted that this enhanced capacity is due to tensile membrane action (TMA), which can be mobilized in the composite slabs at large displacements, irrespective of whether they are restrained or unrestrained horizontally.

A number of studies on tensile membrane behaviour of composite slabs in fire have been conducted, mainly from 1995 to 2003 [1-6], including experimental, numerical, analytical, and design-related research investigations. A design guidance document, SCI publication P288 [7], for steel-framed buildings using composite construction was subsequently developed and applied in the UK. This has allowed structural engineers to take advantage of TMA to minimize the fire protection to interior steel beams and thus to optimize the cost of fire protection. Although previous studies have been very valuable in developing a greater understanding of structural behaviour in fire, most of those from 1995 to 2003 only focused on isolated slab behaviour, rather than on the behaviour of connected floor assemblies.

Recognizing this shortcoming, there has been a recent interest in membrane behaviour of integrated floor assemblies. In 2008, a single composite floor slab panel with two unprotected secondary beams was tested in France [8] as part of the FRACOF project, under exposure to a 120-minute ISO 834 standard fire. The main aim of the test was to assess the fire resistance of a full-scale partially protected floor against the SCI P288 design guidance. All the edge beams were fire-protected, but the two interior secondary beams and the composite slab itself were left unprotected. The results showed a fire resistance, according to the criterion “R” (structural capacity) of over 120 minutes. Also, to assess the suitability of the P288 design rules for use in Germany, Stadler *et al.* [9] conducted two medium-scale tests on composite

beam-slab systems in fire with the aim of investigating the influence of interior supporting beams between two slab panels. They found that tensile membrane forces changed considerably when interior beams were present. Zhang *et al.* [10] conducted furnace tests on four 5.23m x 3.72m composite slabs under ISO 834 standard fire heating, with applied load ratios between 0.6 and 0.65. No structural collapse was seen in these tests. Their observation was that, due to the mobilization of TMA, secondary beams were not needed in supporting the slabs under fire conditions, and therefore these beams could be left unprotected. However, this was not confirmed by the results of a series of tests on composite floor assemblies under fire loading, presented in 2010 by Wellman *et al.* [11]. These were conducted as part of a study intended to consider the elimination of fire protection to interior secondary composite beams in the USA. Partial composite action was achieved in both the main and secondary beams by using headed shear studs. The failure of the edge and interior composite beams was defined as excessive deflection, or excessive deflection rate, according to BS 476 requirements. Based on BS 476 criteria, the observed failure mechanism of the tested specimens was identified as failure of the interior beams, followed by failure of the edge beams. Therefore, the conclusion of the study was not to recommend removal of fire protection from the interior beams of lightweight composite slabs in the context of current construction practice in the USA. This conclusion did not agree with the pre-mentioned tests. This was possibly because the slabs used in these tests were rather thick compared to the span, 101.6mm depth over the shorter span of 2.13m, leading to premature failure of the protected edge beams.

It can be seen from these previous research studies that some important aspects of the system behaviour, such as the effects of unprotected interior beams and of different boundary conditions, on the development of TMA, are still not clearly determined. Thus further

research is required to address the above issues, and this needs to include carefully monitored experimental investigations.

This paper firstly describes an experimental investigation on three one-quarter-scale composite floor assemblies, tested under fire conditions. Specimens, including steel beams, four columns and a concrete slab, were totally enclosed in an electric furnace. The objectives were to study the effects of leaving interior beams unprotected, and of rotational edge-restraint, on the behaviour of composite floor assemblies in fire. The test results have been compared with the Bailey-BRE method used in SCI publication P288, to verify this method for performance-based fire engineering design of composite slab-beam floor systems. A numerical model using ABAQUS/Explicit has also been developed to simulate the tests, and detailed numerical assessments have been conducted.

2 Experimental Programme

2.1 Heating facility

An electric furnace, of length 3m, width 3m and height 0.75m, was designed and commissioned at Nanyang Technological University (NTU); the dimensions were dictated by space constraints within the fire laboratory. Due to limitations on the power supply the furnace could not simulate the ISO 834 standard fire curve. However, in initial trial tests conducted without a specimen, the furnace temperature was able to reach 1000°C within 50 minutes, at a heating rate of about 20°C/min. This temperature increase rate indicates that for actual specimens the heating rate should be within the practical range (5°C/min to 20°C/min) specified for steel sections by BS 5950-8 [12].

2.2 Design of test specimens

The dimensions of the specimens were in turn limited by those of the furnace. Thus the slab dimensions were scaled down to one-quarter of a prototype floor which was designed for

gravity loading at ULS in accordance with EN 1993-1-1 [13] and EN 1994-1-1 [14]. The other parameters, such as beam size, reinforcement ratio, and the ratio of flexural stiffness of the main and secondary beams to that of the slab, were selected so as to closely replicate the relationships typically present in conventional design of composite floors.

Although small-scale tests at elevated temperatures can result in unrealistic temperature distributions in the beams and slabs, the experimental results do provide basic information on the membrane behaviour in fire. They also allow analytical methods and numerical models to be validated; in future work realistic temperature distributions, appropriate to full-scale slab-beam floor systems, can then be incorporated into the validated numerical models.

The three specimens were denoted as S1, S2-FR-IB, and S3-FR. In this nomenclature FR indicates a rotationally restrained system, while IB indicates the presence of interior beams. Specimens S1 and S3-FR were designed without interior beams, while S2-FR-IB (denoted as S2 in a previous conference paper [15]) had two interior beams. The dimensions of all specimens were 2.25m long by 2.25m wide, giving an aspect ratio of 1.0. To simulate interior slab panels, all specimens were designed with a 0.45m outstand beyond the edge beams in both directions, as shown in Fig. 1. In this figure, the notation MB, PSB, and USB denotes a protected main beam, a protected secondary beam, and an unprotected secondary (interior) beam, respectively.

The target thickness h of the slabs was 55mm. Shrinkage reinforcement mesh with a grid size of 80mm x 80mm and a diameter of 3mm (giving a reinforcement ratio of 0.16%) was placed about 38mm below the slab top surface. This 0.16% reinforcement ratio is well within the allowable range specified in EN 1994-1-1 (0.2% for un-propped construction and 0.4% for propped construction). The mesh was continuous across the whole slab, without any laps. The specimens were cast using ready-mixed concrete, with aggregate size ranging from 5 to 10mm, to enable adequate compaction during placement. Specimens S1 and S2-FR-IB were

cast from a single concrete batch, while S3-FR was cast from a separate batch. Thus the mean compressive strengths f_{cm} of the two batches, determined by six cylinder tests 28 days after casting for each batch, differ slightly. Table 1 summarises the properties of the concrete slabs.

Because of the 1:4 scaling there was no standard steel decking suitable for the slabs. To protect the heating elements from concrete spalling, the slabs were cast on a 2.0mm thick steel sheet with small pre-drilled holes. The contribution of this decking to the slab's load-bearing capacity could be ignored, since the unprotected sheet would de-bond from the concrete slab, as observed in previous studies.

All the beams chosen were classified as Class 1 sections according to EN 1993-1-1 [13]. The use of fabricated sections for all secondary beams was necessary, since there was no Universal Beam section suitable for the scaling required. Full-shear composite action between the slab and the downstand beams was achieved by using shear studs of 40mm height and 13mm diameter. The spacing of shear studs was deliberately designed to be close (80mm centre-to-centre), in order to avoid premature failure at the shear studs. This was successful, and no fracture of shear studs, or failure caused by incomplete shear interaction, occurred in any of the three tests. A common type of steel joint (the flexible end plate) was used for both beam-to-beam and beam-to-column connections, as shown in Fig. 2.

Tensile tests were conducted at ambient temperature to obtain the elastic moduli and yield strengths of the beams. For each type of beam section used, four coupons were tested, two from the beam flanges and two from the beam web. Table 2 summarises both the average results from the tensile tests and the measured geometrical properties of the beams.

The experimental program applied the fire protection strategy for members recommended in the SCI P288 publication. The edge beams and columns were protected to a prescriptive

fire-protection rating of 60min. No fire-proofing material was applied to the interior beams or the slabs.

2.3 Test setup and procedure

Fig. 3 shows the final test setup, which consisted of a reaction frame, an electric furnace, a 50-ton hydraulic jack with 450mm available stroke, and a loading system. All gaps between the furnace and the specimen were filled with thermal superwool blanket to reduce heat loss. The test setup was changed for S2-FR-IB and S3-FR to investigate the effect of rotational restraint on the slab-beam behaviour. A restraint system consisting of four 160x100x6 rectangular hollow section (RHS) beams was placed on top of the slab outstands and fixed to the reaction frame via two triangular stiffeners (Fig. 3b). It is assumed that, for all specimens, reinforcement continuity over the supporting protected edge beams and the 0.45-m wide outstands provided little rotational restraint, because only one layer of shrinkage reinforcement was placed inside the slabs. Therefore, slab S1 can be considered as rotationally unrestrained since the outstands can curl upwards reasonably freely. Slabs S2-FR-IB and S3-FR are considered as rotationally restrained by the additional RHS beam system.

The parts of the specimens totally enclosed within the furnace were connected to four fire-protected supporting columns of circular cross-section, using eight M20 bolts to ensure rigid connection between the two parts. These columns were located below and outside the furnace, and connected to the strong floor by hinged connections (Fig. 4). These pin-ended columns allowed the specimen to move horizontally without any restraint, caused no additional bending moments in the slabs, and simplified the test setup.

The concentrated force from the 50-ton hydraulic jack was distributed equally to twelve concentrated point loads by means of a loading system designed to effect a uniform load distribution (Fig. 5). The loading system consisted of three RHS beams and four triangular

steel plates. Between the steel plates and the RHS sections, ball-and-socket joints were used to maintain verticality of the loading system when the slab deformed excessively.

All the specimens were loaded to a value of 15.8kN/m^2 , corresponding to a load ratio of 1.97 for S1 and S3-FR, and 0.43 for S2-FR-IB compared with their low-deflection yield-line failure loads at ambient temperature, which were 8.02kN/m^2 for S1 and S3-FR, and 36.7kN/m^2 for S2-FR-IB. The yield-line load at ambient temperature of S2-FR-IB, calculated with the presence of two interior composite beams, is clearly significantly higher than that of S1 and S3-FR, which have no interior beams.

Transient-state heating was applied. The specimens were first loaded to the predetermined value, heating was then started, and the furnace temperature was increased while the load was manually maintained constant. After failure had been identified the test was ended and the cooling phase took place naturally.

2.4 Acquisition of deformation and temperature measurements

A free-standing outer frame was fabricated and placed around the furnace as a reference support for measurements of displacements during the tests. Twelve linear variable differential transducers (LVDT) were used to measure the vertical displacements of the slabs and the beams, as shown in Fig. 6.

Each specimen was instrumented with 21 K-type thermocouples to capture temperatures at various locations on the slab and beams (Fig. 7). Each member's temperatures were monitored at two or more locations to check temperature uniformity. For the slab, temperatures were measured at the bottom and top surfaces and at the reinforcing mesh level, denoted as SB, ST and S respectively. The beam temperatures were recorded at the bottom and top flanges, and in the web. The thermocouples for beams were denoted as MB, MT and MW for main beams, PB, PT and PW for secondary edge beams, and UB, UT and UW for unprotected secondary beams, respectively. The furnace air temperature was also monitored

by four thermocouples positioned at two side heating panels and two interior positions in the furnace.

3 Experimental Observations and Results

Test results during the heating phase are presented in this paper, because at the end of the loading phase the slab's central residual deflections (measured at LVDT1) were very small, at 2.5mm, 2.7mm and 3.7mm for S1, S2-FR-IB and S3-FR, respectively. Therefore the graphical presentation of results only shows deflections during the heating phase.

The tests were terminated when "failure" occurred. This was defined as the time when either:

- (1) It became inadvisable to allow the slab deflection to develop further, due to the appearance of full-depth cracks, or
- (2) There was a significant drop in the mechanical resistance, and the hydraulic jack could no longer maintain the load level (violation of criterion "*R*").

3.1 Temperature distributions in the slabs

Fig. 8 shows the change of air temperature inside the furnace and the temperatures measured through the slab thickness. These are each the averages of values recorded by three thermocouples at different locations. For example, the temperature at the reinforcing mesh is the average of the values from thermocouples S1 to S3 (Fig. 7). It is shown that the development of air temperature was very consistent up to 45min of heating. Beyond this point there was a small but acceptable deviation of 74°C between the maximum temperature of S1 (909°C) compared to that of S2-FR-IB (983°C). This is because, as the temperature increased, S1 (which allowed the slab outstands to curl upwards) experienced greater heat loss than S2-FR-IB. Test S3-FR was terminated at 59min of heating when failure was identified.

As expected, the temperatures at the slab bottom surface were also consistent among the three tests. However, the temperatures at the mesh and the slab top surface diverged towards the end of the tests, since these temperatures depended not only on the air temperature, but also on the development of through-depth cracks in the concrete. As the slab deflection increased, concrete cracks dispersed differently for the different specimens. On the other hand, the temperatures at the mesh level and the slab's unexposed surface increased slowly, progressing only from 23°C to 120°C within the first 40min. This is because of moisture release from inside the concrete slabs, which slowed down the temperature increase rate during the initial stage. When the free water in the concrete had almost evaporated, the concrete temperatures increased at a greater rate.

3.2 Slab deflections

The relationships between applied load and time are shown in Fig. 9. The designated constant level of applied load for all specimens was 15.8kN/m². Unfortunately, in S1 it was not possible to maintain a constant load level during the heating phase, because of an oil leak during the test. Load had to be reapplied manually to keep it constant. In S2-FR-IB and S3-FR the load was maintained as expected.

Fig. 10 shows comparisons of the mid-span slab deflections, plotted against mesh temperature and time, together with the corresponding failure points. The maximum slab deflections were 131mm, 177mm and 115mm for S1, S2-FR-IB and S3-FR respectively; however, the failure times were very similar, at 86min for S1 and 84min for S2-FR-IB. S3-FR failed very early, at only 45min of heating due to 'brittle' failure as explained in Section 3.5.

Because of the oil leak, S1 experienced a deflection rebound between 30min and 50min of heating. Although the mechanical load reduced significantly during this period, from 15.8kN/m² to 8.16kN/m², the deflection stayed constant. This indicates that thermal effects

(thermal bowing and thermal expansion) were the main factors in controlling the structural response under fire conditions, rather than mechanical load.

As shown in Fig. 10(a), when the mesh temperature was below 100°C S1 and S3-FR experienced similar deflections. This means that at small deflection (below 42 mm), rotational continuity was maintained by the reinforcement over the supporting protected edge beams. Above this temperature, slab S3-FR experienced larger deflection than S1, due to the restraint beam system on top of slab S3-FR. This caused wide cracks to form over the main beams at a very early point, 20min after the start of heating, while these cracks only appeared in S1 after 30min. This demonstrates that the presence of rotational edge-restraint counteracts the increase in the mesh temperature.

The test results are summarized in Table 3. For S1 and S3-FR, the load at the mesh failure temperature $P_{y,\theta_{mesh}}$ is very easy to calculate on the basis of conventional yield-line theory. For S2-FR-IB, it is impossible to determine exactly when the interior beams made no contribution to the yield load. However, at failure of S2-FR-IB (84min), temperature of the unprotected interior beams already reached 892°C at which the reduction factor for yield strength of steel was only 0.064. Therefore, for the purpose of comparison it is reasonable to assume that at the failure of S2-FR-IB, the unprotected interior beams would provide no assistance to the slab capacity. In other words, the yield load of S2-FR-IB at the mesh failure temperature was calculated on the basis of a structural configuration which neglects the interior beams.

3.3 Behaviour of steel frames

3.3.1 Steel beams

Fig. 11, which shows a comparison of the temperature development at the protected beam bottom flanges against time, indicates that the temperature development was very close in all three tests; the differences in the beam behaviour, if any, were not caused by thermal

effects. There was only a slightly difference of the beam temperatures between S1 and S2-FR-IB beyond 60min of heating. This was because S1, which allowed the slab outstands to curl upwards, experienced greater heat loss than S2-FR-IB.

Fig. 12 shows the mid-span deflections measured by LVDT8 and LVDT5 for main beams and protected secondary beams, respectively. For S1 and S2-FR-IB, the deflection-temperature curves can be divided into three phases. In Phase 1, up to 25 minutes of heating (temperatures of about 300°C for main beams and 250°C for protected secondary beams) the beams deflected downwards linearly as a result of thermal bowing. Phase 2 started with a constant deflection rate up to about 420°C for both cases, followed by an increased rate up to 700°C for main beams and 650°C for protected secondary beams. The constant deflection rate can be explained by the decrease of thermal bowing as the temperatures propagated through the slab cross-section. Beyond 450°C the beams gradually lost protection, causing a greater deflection rate. In Phase 3 when the bottom flange temperature was about 700°C for main beams and 650°C for protected secondary beams, the beams showed 'run away' behaviour since at this temperature both the strength and stiffness of the beams had reduced significantly.

However, in S3-FR the deflection-temperature curve for the main beam did not follow this trend. After Phase 1, the main beam of S3-FR showed significant deflection. This was because in S3-FR severe cracks appeared at a very early stage (just 20min after the start of heating) directly above the main beam. Thus composite action between the main beam and the slab could not be maintained, leading to inaccurate measurement of beam deflections, which were obtained from the concrete slab placed directly above the main beam. In contrast, the part of the concrete slab directly above the beams in S1 and S2-FR-IB, as well as that above the protected secondary beams in S3-FR, was fully composite with the beams. Therefore these recorded results are reliable.

After cooling in all the tests, it was observed that local buckling of the beam flanges had not occurred. This could be due to the partial extension of the beams through the flexible end plate connections, in addition to the overall expansion of the slab system.

3.3.2 Steel columns & Connections

Fig. 13 shows the deformed shapes of the protected steel columns after cooling. They indicate that the columns were subjected to biaxial bending due to pulling-in of the edge beam ends at large deflections. Buckling of the column flanges was observed in S2-FR-IB, but was not detected in S1 and S3-FR. This is possibly because in S2-FR-IB, there was greater mobilization of TMA due to unprotected interior beams. This caused greater biaxial bending in the main beams. These bending moments induced greater compression forces for parts of the columns.

None of the connections failed or fractured in any of the tests, during either the heating or the cooling phases. This seems to indicate that, at least where there is limited axial restraint, if the connections are designed accurately in accordance with EN 1993-1-8 [17], and are protected in fire to the same rating as the connected members, composite slabs can mobilise TMA without connection failure during the designated fire period.

3.4 Development of crack patterns in the slabs

The crack pattern development is plotted in Figs. 14-16. The heating times at which cracking occurred are indicated, together with the corresponding temperatures in the reinforcing mesh and the corresponding mid-span slab deflections.

At approximately 10min of heating, diagonal cracks through the slab near the beam-to-column joints started to appear consecutively at the four corners. These cracks developed gradually and opened up through the slab thickness. They occurred in all the tests, and were due to biaxial bending of the outstands. At the slab corners, part of the outstands was in

biaxial bending, but was restrained by the columns, therefore these cracks consistently formed at an angle ranging from 30° to 45° to the slab edges.

After the appearance of the corner cracks, additional cracks formed along the protected edge beams of the slabs; however, the sequence differed between the tests. In S1 and S3-FR, cracks appeared simultaneously along the edge-beam lengths, followed by cracks at the slab centre. In S2-FR-IB, more severe cracks were observed, first above the main beams and then in the vicinity of the protected secondary beams. Cracks along the unprotected secondary beams appeared near to the end of the test. During this test, minor cracks appeared at the mid-span of S2-FR-IB. These cracks had closed up after the test, possibly because of the rebound of deflection during cooling. These different sequences of crack development can be attributed to the different load paths from the slabs to the protected edge beams, as will be explained in Section 5.1.

For S1 and S3-FR, after 30min of heating, the compression ring began to form when the mesh temperature had reached about 100°C. The corresponding deflections were 42mm and 52mm, equal to 0.8 and 0.95 of the slab thickness respectively. For S2-FR-IB, after 50min of heating the compression ring began to form at a mesh temperature of 220°C. The corresponding deflection was 52mm, or 0.95 of the slab thickness. It is obvious that S2-FR-IB, which had interior beams, entered the tensile membrane action stage later than S1 and S3-FR, because the unprotected secondary beams enhanced the slab capacity during the bending stage. It is noticeable that TMA was mobilised in each case at a deflection approximately equal to 0.95 of the slab thickness, irrespective of the presence of interior beams.

3.5 Failure modes

In S1, concrete cracking occurred around the column locations; however the test was continued, since there was no obvious indication of failure. After 72min of heating, a single-curvature folding mechanism at the slab mid-span, including the formation of plastic hinges

in the protected secondary beams, was observed and is shown in Fig. 17(a). At this stage, when the beam temperature had already reached 692°C, the residual bending resistance of the protected secondary beams (calculated as a composite beam) at the mid-span section was 22.2kNm, which was smaller than the applied bending moment of 32.0kNm due to the mechanical load of 15.64kN/m² and difference in temperatures of the beam top and bottom fibres. After 86min of heating there was a loud sound caused by fracture of reinforcement. Two full-depth cracks were observed; one close to a main beam and the other directly above a protected secondary beam (Fig. 17(b)). Heating was stopped at this point, and no controlled cooling was conducted.

Test S2-FR-IB ended when fracture of reinforcement occurred and full-depth cracks appeared close to the edge beams, as shown in Fig. 18(a). However, no folding mechanism was observed. This may be due to the presence of interior beams and the rotational restraint beams on top of the slab, which prevented single-curvature folding.

In S3-FR, a compression ring formed after 28min of heating with the appearance of curved cracks at the four corners (Fig. 19(a)). However, at 45min three full-depth cracks appeared suddenly; one at the slab corner near the steel column, and two above the main beams. These cracks led to a 'brittle' failure of the compression ring and caused 'run-away' behaviour in the slab. The supporting compression ring could no longer be maintained, and therefore TMA was not able to develop further.

In summary, the failure modes observed included:

- (a) Fracture of reinforcement close to the protected edge beams (all tests);
- (b) Folding in single-curvature, by formation of plastic hinges in the secondary edge beams (S1) and a yield line across the slab;
- (c) Compression ring failure (S3-FR). No global collapse was observed.

These failure modes differ in some respects from those considered in the SCI P288 design guide. In P288 the two common failure modes are fracture of reinforcement across the short span at the slab mid-span and compressive failure of the concrete at the slab corners. However, in the authors' tests no fracture of reinforcement at mid-span was observed, although cracks appeared at the slab centre. This is because the observed failure modes in these tests are composite beam-slab collapse mechanisms, not TMA mechanism in the slabs.

4 Finite element analysis

In this section the modelling techniques, including the types of elements used, the boundary conditions and material models, are described. A commercially available finite element program ABAQUS [18] was used to develop the finite-element (FE) model. This FE model was then validated against the test results, in terms of thermal and structural deflection responses, and failure modes. The model was then used to provide insight into stress distribution. It can be seen that the FE models show considerable accuracy in simulating the structural behaviour.

4.1 Modelling technique

The *Sequentially coupled thermal-stress analysis procedure* in ABAQUS/Explicit was used because, while the thermal field is the major driver for the stress analysis, the thermal solution does not depend on the stress solution. The *Concrete damaged plasticity model* was adopted, and reinforcement was modelled using the layered rebar technique. With regard to concrete damaged plasticity model, there is no fixed maximum concrete strain in both tension and compression. For compression hardening, ABAQUS suggests that the maximum strain should be calibrated to a particular case. Therefore, the compressive inelastic strains for concrete in compression, the concrete strain $\varepsilon_{cu,\theta}$ corresponding to $f_{c,\theta}$ and the maximum concrete strain $\varepsilon_{ce,\theta}$, were taken from EN 1994-1-2 [14]. For tension stiffening, to avoid

potential numerical problems, ABAQUS enforces a lower limit on the post-failure stress equal to one hundred of the initial failure stress: $\sigma_t \geq \sigma_{t,0}/100$. Thus, if the tensile concrete stress is approximately equal to this limit, the concrete can be considered as failure.

A four-noded doubly-curved thin or thick shell element with reduced integration, the S4R shell element, was used to discretize both the beams and the slab. The beam top flange and parts of the slab above the beams were tied together using surface-based contact interactions to simulate fully composite action between the steel downstand beams and the slab. An offset between the two tied surfaces was adopted to avoid any overlap between the two reference surfaces. This form of modelling assumed perfect bonding between the steel beam and the concrete slab.

Material properties of the steel and the concrete were obtained from tensile coupon tests and concrete cylinder tests conducted at ambient temperature. The material properties at elevated temperatures were then deduced using the material reduction factors specified in EN 1994-1-2 [19]. For steel materials, the stress-hardening part was taken into account, and the strain parameters were assumed to take the values recommended in EN 1994-1-2. Therefore, in the fire situation, the limiting strain for yield strength $\varepsilon_{au,\theta}$ was taken as 0.15, and the ultimate strain in the fire situation $\varepsilon_{ae,\theta}$ as 0.2.

Fig. 20 shows a simplified one-quarter numerical model (double symmetry), taking into account the protected and unprotected steel beams, the concrete slab, and the reinforcing mesh. Vertical support to the slab edges was provided by the protected edge beams. In turn, these beams were supported by the stocky columns. Thus vertical restraint ($U3 = 0$) was imposed at the column connection locations; it is assumed that the vertical displacement at these positions is negligible. This assumption is reasonable, because the maximum recorded vertical displacement at the column support positions was only 3.1mm in S3-FR. Unfortunately, this value was not measured in S1 and S2-FR-IB. The FE model had been

validated with good agreement against the FRACOF test results [8, 20]. For S2-FR-IB and S3-FR, vertical restraint along the edge outstands was used to model the rotational restraint beam system; no springs were needed to model this beam system.

The recorded temperatures across the beam sections were entered directly into the numerical model. For the slabs, the measured temperatures at the slab bottom surface were input, and then thermal gradient over the slab depth was identified.

4.2 Results

4.2.1 Comparisons of slab deflection and temperature development

Figs. 21-23 provide comparisons of temperature distribution and deflections of the slab and beams between the FE analyses and the experimental results. With a thermal gradient of $10^{\circ}\text{C}/\text{mm}$ the predicted temperatures were very close to the recorded ones, except for the mesh temperature in S3-FR (Fig. 23(a)). This is because, in S3-FR, severe cracks appeared over the perimeter of protected beams, rapidly leading to significant heat loss. As a result, the recorded mesh temperature increased at a lower rate after the cracks had appeared. The mesh temperature in S3-FR only increased from 91°C (after 22.5min of heating) after cracks appeared to 150°C (after 45min of heating).

As shown in Figs. 21(b)-23(b), generally the numerical predictions match well with the test results. The discrepancies in the slab deflection curves between the predicted and experimental results after the mesh temperature reached 200°C for S1, and 100°C for S3-FR, are attributed to two reasons. Firstly, as the deflection increased, cracks in the concrete slabs developed, leading to significant heat loss. However, the numerical model can not simulate this phenomenon, resulting in greater prediction of mesh temperature. Secondly, the numerical model cannot predict concrete spalling, which had a significant effect on the slab behaviour. In S2-FR-IB the cracks were not as severe as those in S1 and S3-FR, and so the prediction for this test is considerably better.

4.2.2 Comparisons of the displacement of the edge beams against temperature

The results in terms of beam deflections versus temperature (Figs. 21(b)-23(b)) show that in general the model predicts the beam behaviour very well. For the main beam of S3-FR, although the trend was similar, the comparison is poorer because severe cracks appeared directly above the main beam top flange, leading to greater inaccuracy in the measurements.

4.2.3 Failure modes & Stress distribution

Figs. 24-26 show the stress distributions across the sections and at the top surfaces of the slabs at failure. In these figures, 'Section 1' denotes the mid-span section perpendicular to the protected secondary beams, 'Section 2' denotes the mid-span section perpendicular to the main beams, 'OverMB' is the cross-section above a main beam, and 'OverPSB' is the cross-section above a protected secondary beam. The positions of these sections are indicated in Figs. 24(b)-26(b).

It can be seen that, for S1 at 85.6min, the highest tensile stress in the reinforcing mesh across a protected secondary edge beam is higher than that across the mid-span section (511MPa compared to 487MPa on Section 2). For S2-FR-IB at 84.0min, the maximum tensile stress of 377MPa is located above the main beam, while the maximum stress in the reinforcement across the slab mid-span (Section 1) is 330MPa. For S3-FR, the maximum tensile stress of 659MPa is found at the slab mid-span (Section 2), followed by that above the protected secondary beam (638MPa). Therefore, on the basis of numerical simulations, in S1 and S2-FR-IB the fracture of reinforcement above the edge beams would occur first, before the fracture of reinforcement at the mid-span of the slabs. This observed failure mode in the model concurs with experimental observations. In S3-FR predicted failure is due to fracture of reinforcement at the slab mid-span; however, in the actual test, the failure mode was due to failure of the compression ring. As shown in Table 4, the equivalent plastic strains in uniaxial compression (PEEQ) at the slab top surfaces at its corners are 0.0057, 0.0031 and 0.0051, for

S1, S2-FR-IB and S3-FR respectively. These values are approximately equal to the compressive strain $\varepsilon_{cu,\theta}$ (which corresponds to $f_{c,\theta}$) according to EN 1994-1-2 [19], which would have been 0.0051, 0.0039 and 0.0033, for S1, S2-FR-IB and S3-FR, respectively at the prevailing temperature of the concrete slab. It should be noted that the equivalent plastic strains of S1 and S3-FR have exceeded the compressive strain $\varepsilon_{cu,\theta}$. This means that the failure has occurred at the slab corners for S1 and S3-FR, but not for S2-FR-IB. Unfortunately, there is no obvious indication of which failure mode occurred first, and it seems that fracture of the reinforcement is the most likely failure mode for slabs having interior beams.

The principal stress distributions at the top surface of the slabs are shown in Figs. 24(b)-26(b), in which negative values indicate compressive stresses and positive values indicate tensile stresses. It can be seen that TMA was clearly mobilized in all specimens, with the formation of a tensile zone at the slab centre and a peripheral 'compression ring'. The compression ring consists of part of the concrete slab above the edge beams and part of the top flange of the edge beams.

5 Discussion

Results and observations from an experimental programme consisting of three one-quarter scale tests on composite slab-beam systems in fire have been presented in this paper. Two of the slabs (S1 and S3-FR) did not have interior composite beams; the other (S2-FR-IB) had two interior beams. The test setup was varied in order to investigate the effect of rotational edge-restraint on the slab behaviour.

5.1 Effect of interior beams

As shown in Fig. 10(a), S2-FR-IB failed at a deflection of 177mm when the mesh temperature had reached 512°C. The corresponding values were 131mm at 391°C and

115mm at 150°C, for S1 and S3-FR respectively. On the other hand, Table 3 indicates that S2-FR-IB had the greatest enhancement factor, at 2.55 compared to 1.96 for S1 and 1.54 for S3-FR. This enhancement factor is defined in this paper as the ratio of the test failure load to the small-deflection yield-line failure load at the same mesh temperature. It is obvious that continuity of reinforcement over supporting beams, and the presence of interior beams, have significantly reduced the slab deflection and enhanced the slab's load-bearing capacity. The enhanced capacity is greatly assisted by the tensile forces created in the interior beams, as observed in Fig. 25(b).

The interior beams also considerably affect the magnitude of stress in the mesh reinforcement, as well as its distribution, and this may have led to differences in the failure modes of the floor assemblies. As can be seen in Figs. 24(a)-26(a), in the case of S2-FR-IB the maximum tensile stress in the reinforcement across the mid-span cross sections was only 330MPa, which is smaller than the reinforcement stress above the edge beams. In contrast, the corresponding values were 487MPa and 659MPa, for S1 and S3-FR respectively; these are both greater than the reinforcement stress above the edge beams. Consequently, the failure mode may change from reinforcement fracture at mid-span (for cases without interior beams) to reinforcement fracture in the vicinity of edge beams (for cases with interior beams).

The difference in the stress distributions can be clearly identified in Figs. 24(b)-26(b). For S2-FR-IB, the tensile stresses caused by TMA in the reinforcement above the interior beams are reduced, partly because of the superposed compressive stresses caused by sagging bending of the T-flange composite interior beams. For S1 and S3-FR with no interior beams, the tensile stresses are continuous with the maximum values at the centres of the slabs.

The effect of interior beams on the deflection of edge beams can be deduced from Fig. 12. At similar temperatures, with the same test setup, the protected secondary beams of S3-

FR had a greater deflection than those in S2-FR-IB, because of the difference in load path from the slabs to the beams. During the initial heating stage, in S3-FR load was transferred directly to the protected edge beams, while in S2-FR-IB the load was transferred via unprotected interior beams to the protected edge beams. As temperatures increased, the load transfer mechanism of the two slabs became the same, since the unprotected interior beams progressively lost both stiffness and strength from 400°C onwards. Also, the main beam of S2-FR-IB had a slightly greater deflection than that of S1 because of the difference in load paths as described above.

5.2 Effect of rotational restraint

As can be seen in Figs. 24(a) and 26(a), the maximum stresses in the reinforcement above the edge beams were significantly greater in S3-FR at 45min of heating than those in S1 at 85.6min of heating. The maximum stresses in the reinforcement over protected secondary and main beams in S3-FR were 638MPa and 614MPa respectively, while the corresponding values in S1 were only 511MPa and 482MPa respectively. This can be explained by the effect of rotational restraint on the stress distribution; where rotational restraint exists, stresses above the edge beams are more intense. This results in severe concrete crushing at the four corners and wide tension cracks over the edge beams. Thus the failure of the compression ring occurred quickly in S3-FR. Once the compression ring failed, the TMA mechanism could not be sustained, and consequently the slab failed.

Comparisons of beam deflection between S1 and S3-FR are shown in Fig. 12. It should be noted that the outstands of S1 were able to curl upwards freely, but in S3-FR this was not possible due to external restraint. It can be seen that the rotational restraint has no effect on the vertical displacement of the main beams. On the other hand, the PSB deflections of S3-FR were greater than those of S1. This may be attributed to the additional mechanical load of the outstands applied to the protected secondary beams of S3-FR due to external restraint.

6 Conclusions

An experimental study has been conducted on reduced-scale composite slab-beam systems under fire conditions, in order to study their structural behaviour. Additionally, FE models using ABAQUS/Explicit software have been developed to simulate the tests. On the basis of the experimental results and the numerical evaluations, the following conclusions can be drawn:

- (1) Both reinforcement continuity over the supporting edge-beams, and the presence of interior beams, can reduce deflections and greatly enhance the load-bearing capacity of these slab-beam systems. The observed enhancement factors were 1.96, 2.55, and 1.54 above the yield line capacity for S1, S2-FR-IB and S3-FR, respectively.
- (2) Slabs with interior beams enter the tensile membrane action stage later than slabs without interior beams, because these interior beams enhance the slab capacity due to bending resistance.
- (3) The presence of interior beams significantly affects the magnitude, as well as the distribution of stress in the mesh reinforcement. The maximum tensile stresses did not necessarily occur at the slab centre, but could be located in the concrete slab above the protected edge beams. This may cause different failure modes for floor assemblies, compared with isolated slab panels.
- (4) Rotational restraint induces intense stress concentration above the edge beams, which can result in premature concrete crushing at the four corners and wide cracks over the edge beams. The rotational restraint did not have any significant effect on the beams' vertical deflections.
- (5) The test specimens revealed different 'composite beam' failure modes of the floor assemblies. These include: (a) fracture of reinforcement in the vicinity of protected edge beams; (b) in cases without unprotected interior beams, failure occurred through

crushing of compression ring (S3-FR test) or folding in single-curvature by formation of plastic hinges in the secondary edge beams (S1 test). No fracture of reinforcement was observed at the mid-span of the slabs.

- (6) Irrespective of the presence of interior beams, tensile membrane action is mobilised at a deflection equal to approximately 0.9 to 1.0 of the slab thickness.
- (7) None of the connections failed or fractured during either the heating or cooling phases.
- (8) The accuracy of a FE model in predicting the behaviour of the composite slab-beam systems at large deflections is controlled by the accuracy of prediction of the temperature of the mesh reinforcement.

Acknowledgment

*The research presented in this paper was funded by Agency for Science, Technology and Research (A*Star Singapore). The financial support of A*Star is gratefully acknowledged.*

REFERENCES

- [1] Bailey CG, Toh WS. Small-scale concrete slab tests at ambient and elevated temperatures. *Engineering Structures*. 2007;29:2775-91.
- [2] Huang ZH, Burgess IW, Plank RJ. Modelling membrane action of concrete slabs in composite buildings in fire. I: Theoretical development. *J Struct Eng-ASCE*. 2003;129:1093-102.
- [3] Izzuddin BA, Elghazouli AY. Failure of lightly reinforced concrete members under fire. I: Analytical modeling. *J Struct Eng-ASCE*. 2004;130:3-17.
- [4] Bailey CG, White DS, Moore DB. The tensile membrane action of unrestrained composite slabs simulated under fire conditions. *Engineering Structures*. 2000;22:1583-95.
- [5] Bailey CG, Moore DB. Structural behaviour of steel frames with composite floor slabs subject to fire: Part 1: Theory. *The Structural Engineer*. 2000;78:19-27.
- [6] Bailey CG, Moore DB. Structural behaviour of steel frames with composite floorslabs subject to fire: Part 2: Design. *The Structural Engineer*. 2000;78:28-33.
- [7] Newman GM, Robinson JT, Bailey CG. *Fire Safe Design: A new Approach to Multi-Story Steel-Framed Buildings*. 2nd ed: The Steel Construction Institute; 2006. SCI Publication P288.
- [8] Zhao B, Roosefid M, Vassart O. Full scale test of a steel and concrete composite floor exposed to ISO fire. *Proceedings of the Fifth International Conference on Structures in Fire (SiF'08)*. Singapore: Nanyang Technological University; 2008:539-50.
- [9] Stadler M, Mensinger M, Schaumann P, Sothmann J. Munich Fire Tests on Membrane Action of Composite Slabs in Fire - Test Results and Recent Findings. *Applications of Structural Fire Engineering*. Prague, Czech Republic 2011.
- [10] Zhang N-S, Li G-Q, Lou G-B, Jiang S-C, Hao K-C. Experimental study on full scale composite floor slabs under fire condition. *Applications of Structural Fire Engineering*. Prague, Czech Republic 2009: 502-11.
- [11] Wellman E, Varma A, Fike R, Kodur V. Experimental Evaluation of Thin Composite Floor Assemblies under Fire Loading. *J Struct Eng-ASCE*. 2011:1002-12.
- [12] BS 5950-8: *Structural use of steelwork in building. Part 8: Code of practice for fire resistant design*. British Standards Institution (BSI), London, 2003.
- [13] EN 1993-1-1: *Eurocode 3. Design of Steel Structures. Part 1-1: General Rules and Rules for Buildings*. European Committee for Standardization (CEN), Brussels, 2005.
- [14] EN 1994-1-1: *Eurocode 4. Design of Composite Steel and Concrete Structures. Part 1-1: General Rules and Rules for Buildings*. European Committee for Standardization (CEN), Brussels, 2004.

- [15] Nguyen TT, Tan KH. Testing of Composite Slab-beam Systems at Elevated Temperatures. *7th International Conference on Structures in Fire (SiF)*, Zurich, Switzerland. 2012: 247-56.
- [16] EN 1992-1-1: *Eurocode 2. Design of Concrete Structures. Part 1-1: General Rules and Rules for Buildings*. European Committee for Standardization (CEN), Brussels, 2004.
- [17] EN 1993-1-8: *Eurocode 3. Design of Steel Structures. Part 1-8: Design of joints*. European Committee for Standardization (CEN), Brussels, 2005.
- [18] ABAQUS/CAE User's Manual 6.9: Dassault Systèmes Simulia Corp., Providence, RI, USA; 2009.
- [19] EN 1994-1-2: *Eurocode 4. Design of composite steel and concrete structures. Part 1-2: General Rules - Structural fire design*. European Committee for Standardization (CEN), Brussels, 2005.
- [20] Nguyen TT, Tan KH. Numerical Investigations of Composite Slab-Beam Floor Systems Exposed to ISO Fire. *Applications of Structural Fire Engineering*. Prague, Czech Republic, 2011.
- [21] Bailey CG, Toh WS. Behaviour of concrete floor slabs at ambient and elevated temperatures. *Fire Safety Journal*. 2007;42:425-36.

Journal:

**Behaviour of Composite Slab-Beam Systems at Elevated Temperatures:
Experimental and Numerical Investigation**

List of Tables

Table 1 Properties of concrete slabs

Table 2 Properties of I-section beams

Table 3 Summary of test results

Table 4 Strains at the top surface of the slabs based on FE analyses

Table 1 Properties of concrete slabs

	h mm	d_x mm	d_y mm	f_{cm} MPa	f_{ctm} MPa	Elastic	f_y / f_u MPa	Elong	Elastic
						Modulus E_{cm} , GPa		ation %	Modulus E_s , MPa
S1	55	35	38	36.3	2.8	32.4	543/771	22.2	180000
S2-FR-IB	55	35	38	36.3	2.8	32.4	543/771	22.2	180000
S3-FR	58	37	40	31.3	2.4	31.0	648/806	14.8	203352

Table 2 Properties of I-section beams

Specimens		Depth	Width	Thickness		Yield stress	Ultimate stress	Elastic modulus
		h (mm)	b_f (mm)	Web t_w (mm)	Flange t_f (mm)	f_y (MPa)	f_u (MPa)	E_s (MPa)
		S1 &	MB	131	128	6.96	10.77	302
S2-FR-IB	PSB & USB	80	80	9.01	9.14	435	533	206900
	UC	157.6	153	6.90	9.70	321	489	196698
S3-FR	MB	131	128	6.97	11.03	307	462	211364
	PSB & USB	80	80	10.26	10.02	467	588	210645
	UC	157.6	153	6.90	9.70	321	489	196698

Table 3 Summary of test results

Specimen	Thickness d	$P_{y,20}$	Time violated 'R' criterion	Failure Temperature ($^{\circ}\text{C}$)			P_{test}	Load ratio	$P_{y,\theta_{mesh}}$	Maximum deflection δ_I	δ_I/d	Enhancement factor $e_{test} = P_{test} / P_{y,\theta_{mesh}}$
				θ_{top}	θ_{mesh}	θ_{bottom}						
S1	55	8.0	85.8	172	391	630	15.62	1.95	7.97	131	2.38	1.96
S2-FR-IB	55	36.8	84.0	95	512	664	15.13	0.41	5.93	177	3.22	2.55
S3-FR	58	10.4	45.0	60	150	351	15.98	1.54	10.35	115	1.98	1.54

Table 4 Strains at top surface of the slabs based on FE analyses

	Failure time	Equivalent plastic strain in uniaxial compression at corners	Temperature at top surface ($^{\circ}\text{C}$)	Compressive strain $\epsilon_{cu,\theta}$ corresponding to $f_{c,\theta}$ in EN 1992-1-2	Maximum concrete strain $\epsilon_{ce,\theta}$ in EN 1992-1-2
S1	85.8	0.0057	172	0.0051	0.0243
S2-FR-IB	84.0	0.0031	95	0.0039	0.0223
S3-FR	45.0	0.0051	60	0.0033	0.0213

List of Figures

Fig. 1 Structural layout of the specimens

Fig. 2 Flexible end plate connections

Fig. 3 Final test setup

Fig. 4 Supporting columns

Fig. 5 Loading point positions

Fig. 6 Arrangement of LVDT

Fig. 7 Arrangement of thermocouples

Fig. 8 Air temperature and temperature distributions over slab thickness

Fig. 9 Load – time relationship

Fig. 10 Mid-span slab deflection vs. Mesh temperature and Time

Fig. 12 Mid-span deflection of main beam (MB) and protected secondary beam (PSB)

Fig. 13 Deformed shapes of columns after tests

Fig. 14 Development of crack pattern of S1

Fig. 15 Development of crack pattern of S2-FR-IB

Fig. 16 Development of crack pattern of S3-FR

Fig. 17 Failure mode of S1

Fig. 18 Failure mode of S2-FR-IB

Fig. 19 Failure mode of S3-FR

Fig. 20 Typical quarter FE model

Fig. 21 Comparisons between simulation and test for S1

Fig. 22 Comparisons between simulation and test for S2-FR-IB

Fig. 23 Comparisons between simulation and test for S3-FR

Fig. 24 Numerical results of S1 at failure – 85.6 min

Fig. 25 Numerical results of S2-FR-IB at failure – 84.0 min

Fig. 26 Numerical results of S3-FR at failure – 45.0 min

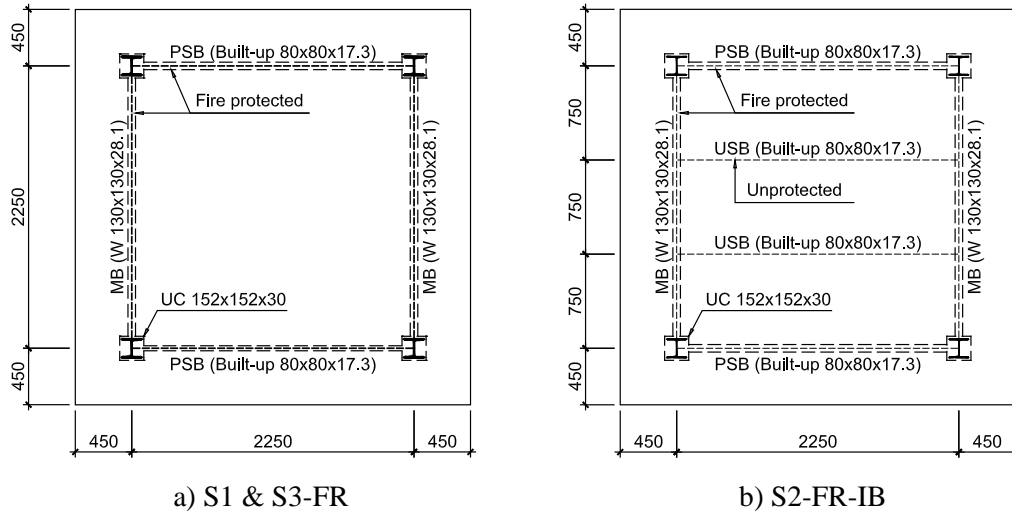


Fig. 1 Structural layout of the specimens

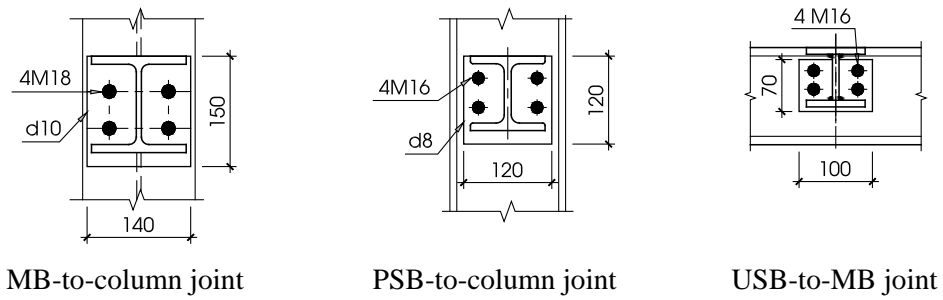


Fig. 2 Flexible end plate connections

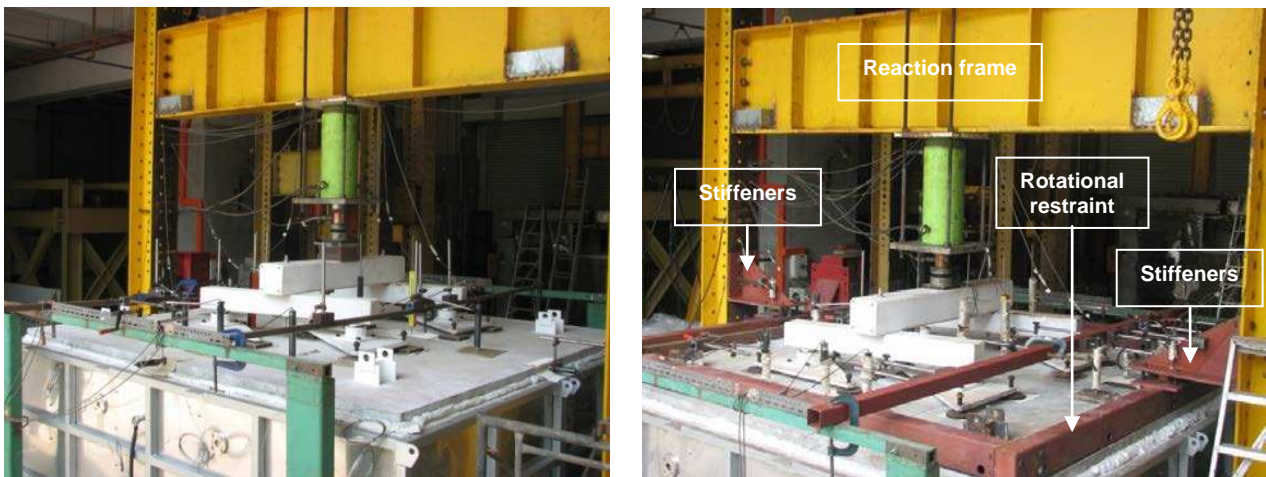


Fig. 3 Final test setup



Fig. 4 Supporting columns

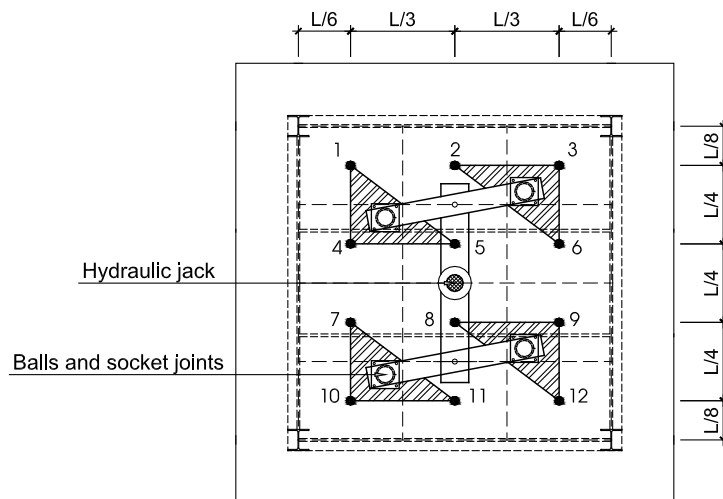


Fig. 5 Loading point positions

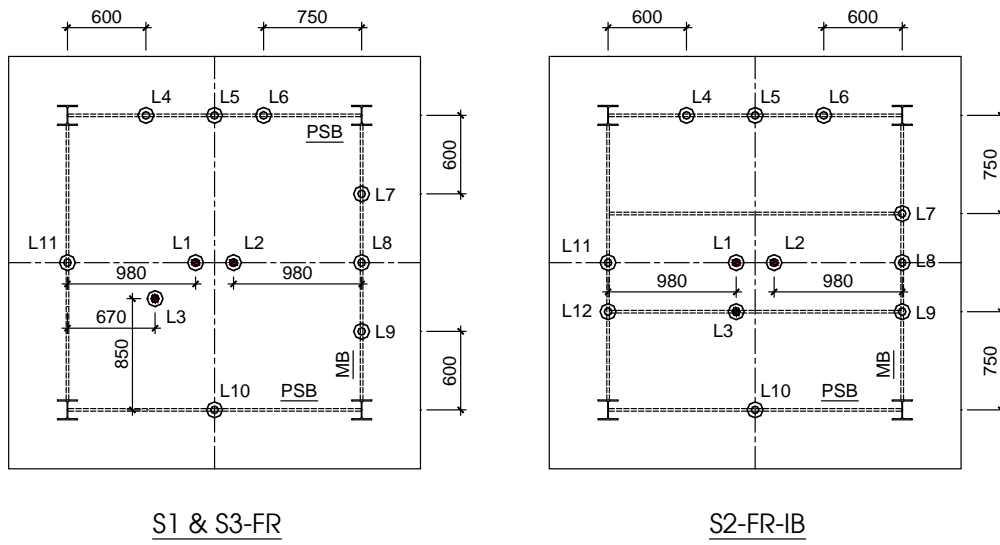


Fig. 6 Arrangement of LVDT

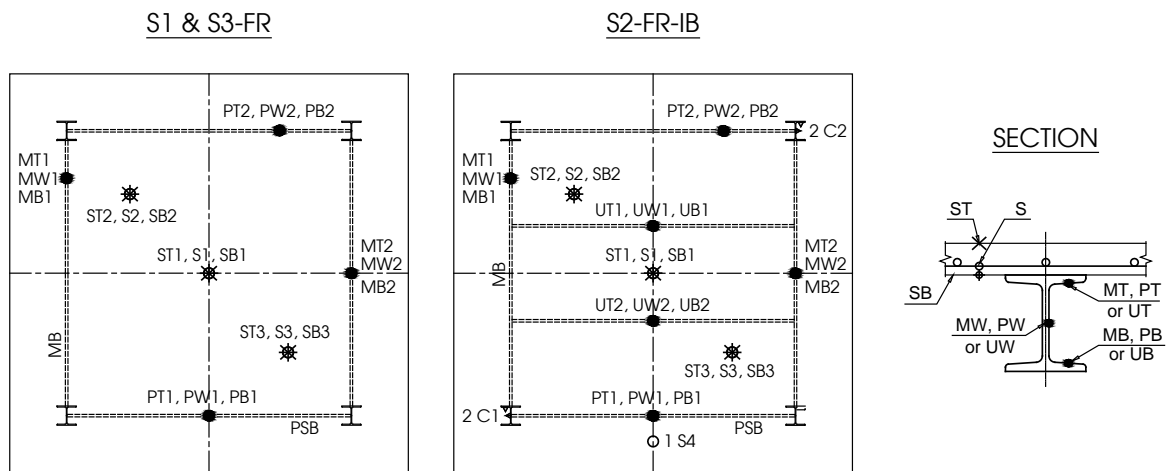


Fig. 7 Arrangement of thermocouples

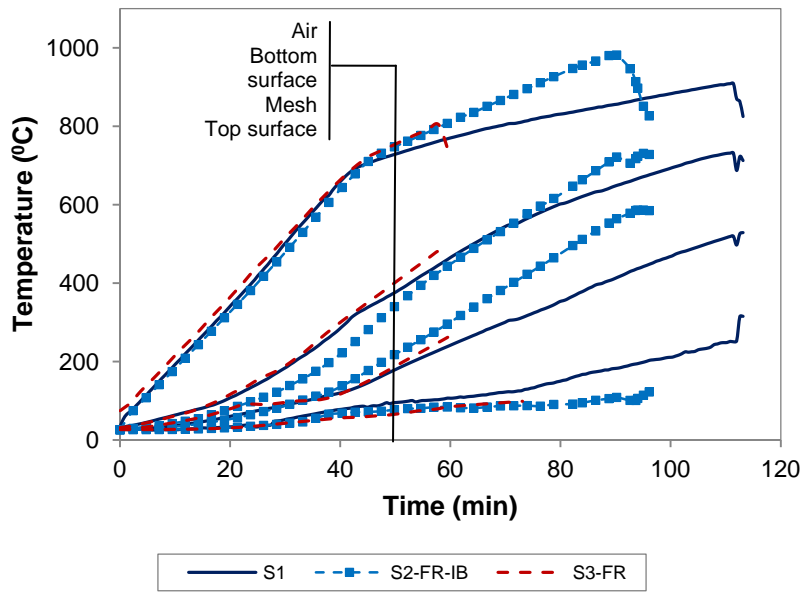


Fig. 8 Air temperature and temperature distributions over slab thickness

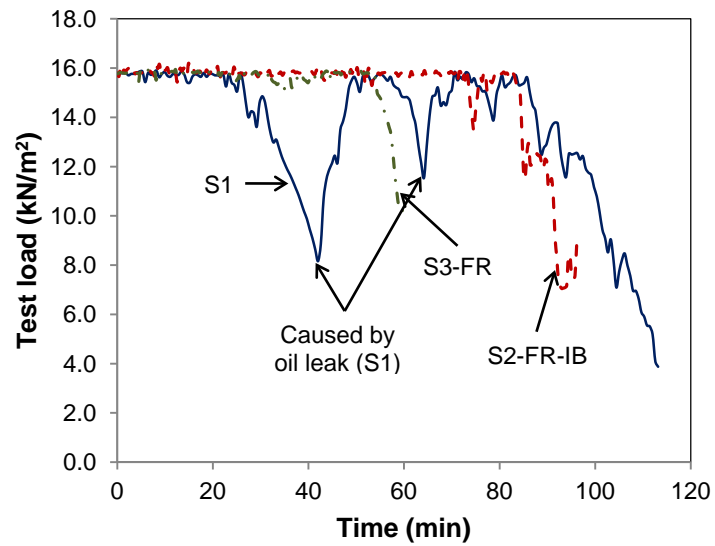
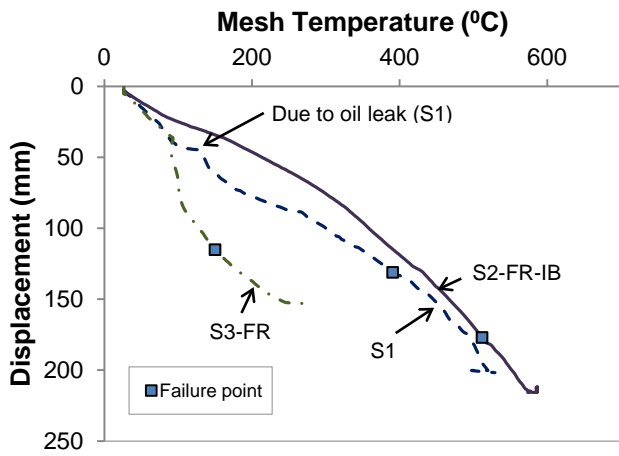
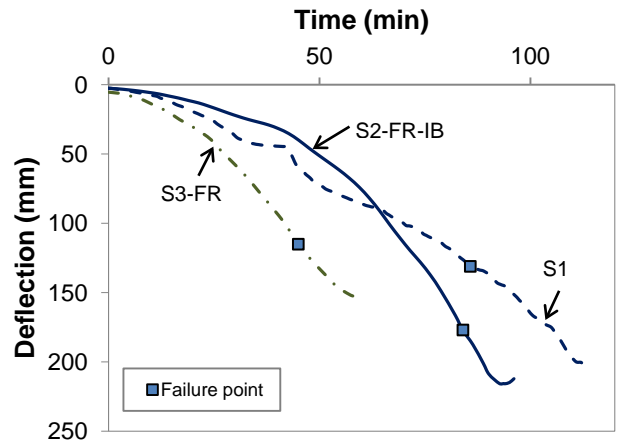


Fig. 9 Load – time relationship



a) Deflection vs. Mesh temperature



b) Deflection vs. Time

Fig. 10 Mid-span slab deflection vs. Mesh temperature and Time

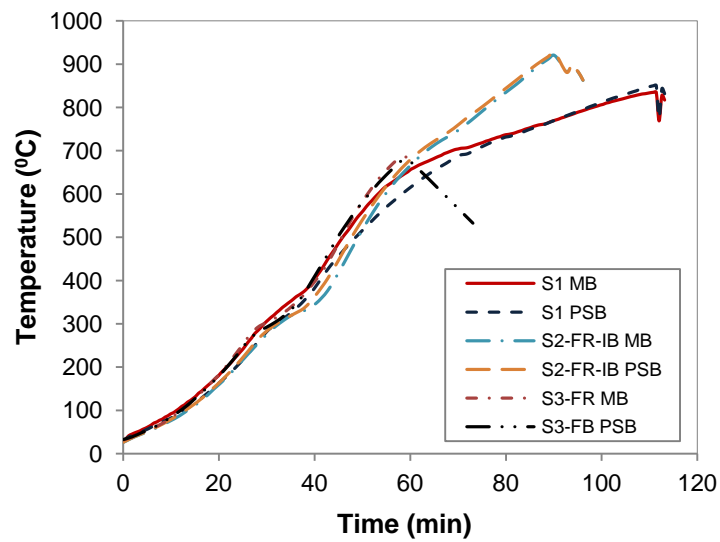


Fig. 11 Temperature developments at beam bottom flanges

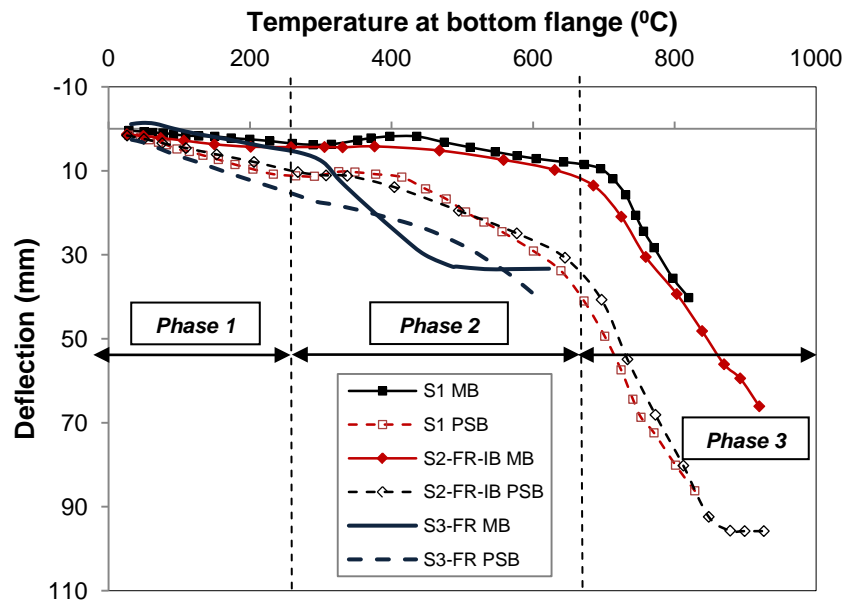


Fig. 12 Mid-span deflection of main beam (MB) and protected secondary beam (PSB)



S1

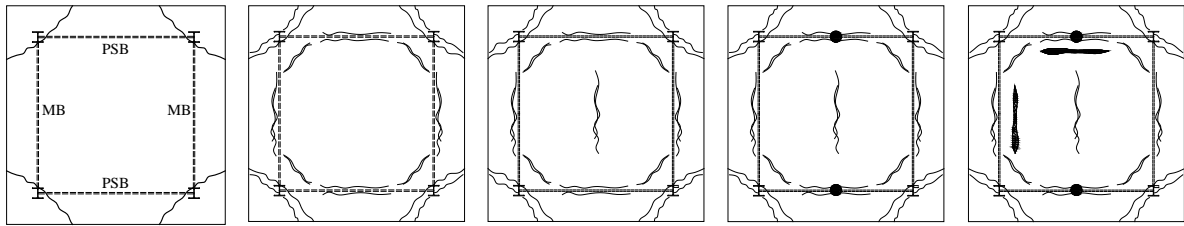


S2-FR-IB



S3-FR

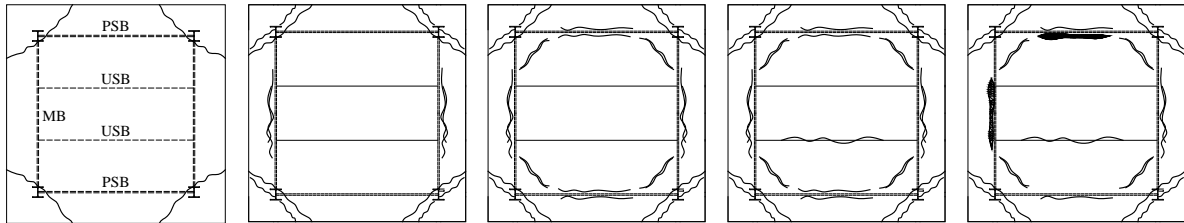
Fig. 13 Deformed shapes of columns after tests



12min – 48°C 30min – 100°C 53min – 221°C 65min – 294°C 86min – 390°C
 14mm 42.3mm (*) 81.8mm 97.8mm 135mm

- Plastic hinges in beams ; (*) Compression ring formed

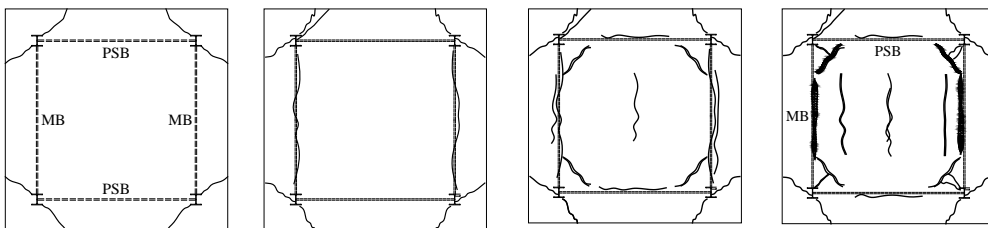
Fig. 14 Development of crack pattern of S1



15min – 42°C 35min – 111°C 50min – 220°C 60min – 302°C 84min – 512°C
 8.6mm 26.9mm 51.8mm (*) 76.3mm 177mm

- (*) Compression ring formed

Fig. 15 Development of crack pattern of S2-FR-IB



17min – 66°C 18min – 71°C 28min – 93°C 45min – 152°C
 25.2mm 27.3mm 52mm (*) 116.2mm

- (*) Compression ring formed

Fig. 16 Development of crack pattern of S3-FR



a) Folding mechanism



b) Failure mode

Fig. 17 Failure mode of S1



a) Crack pattern



b) Fracture of reinforcement

Fig. 18 Failure mode of S2-FR-IB



a) Crack pattern



b) Compressive ring failure

Fig. 19 Failure mode of S3-FR

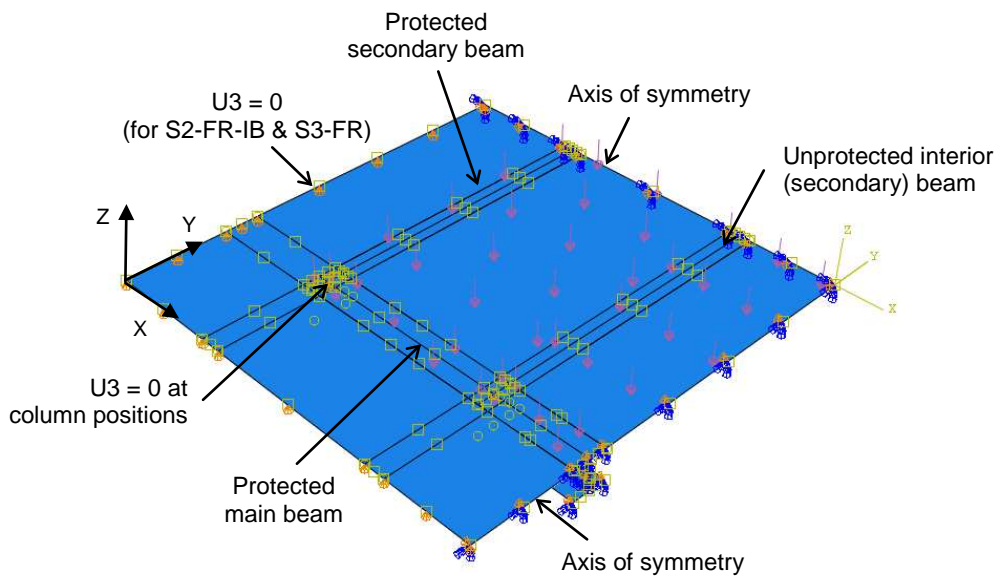
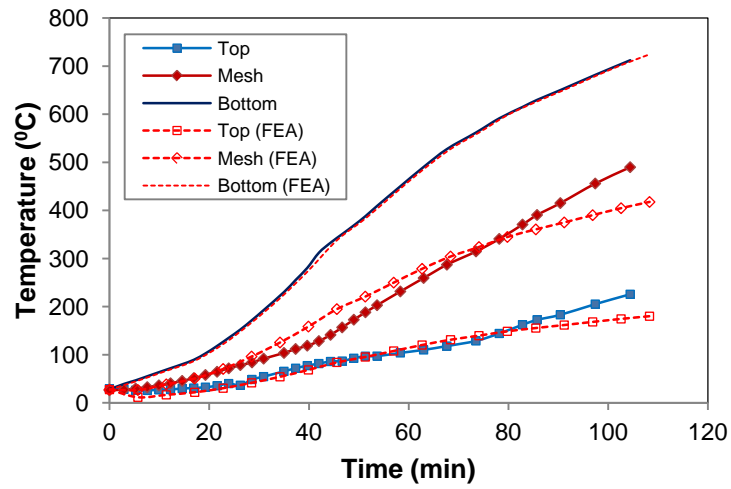
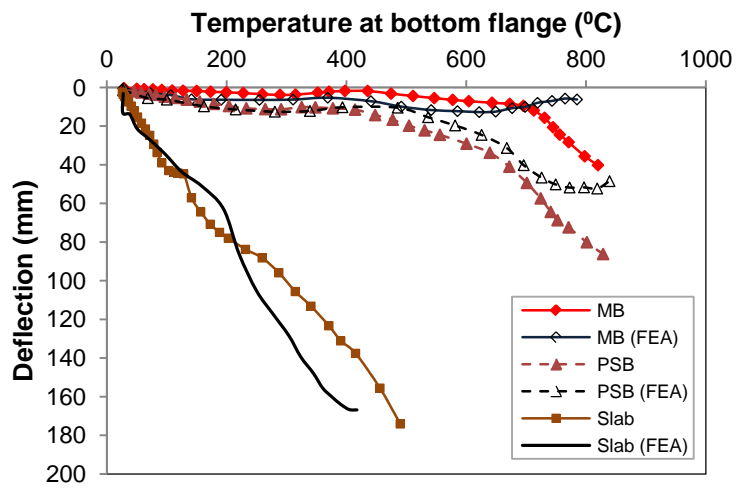


Fig. 20 Typical quarter FE model

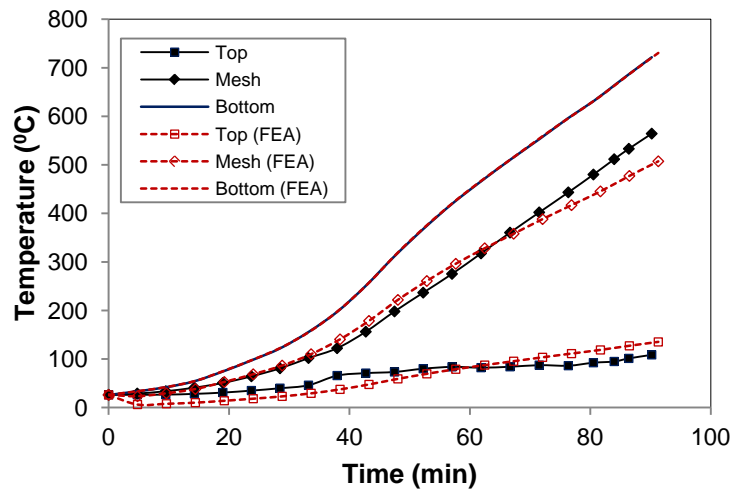


a) Temperature distribution of slab

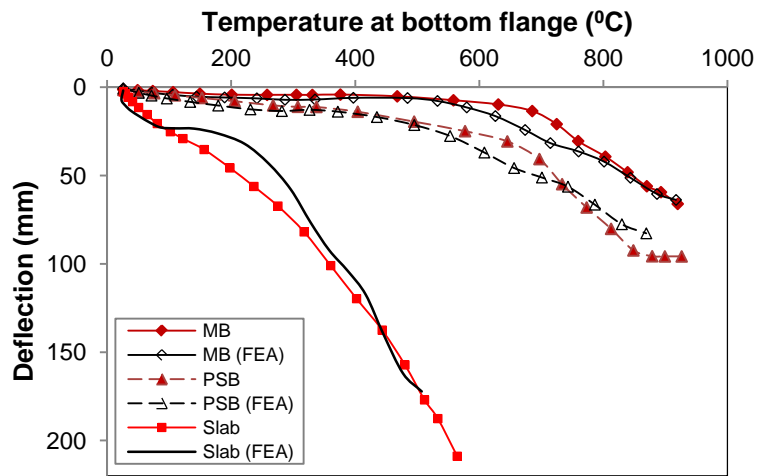


b) Deflection comparison

Fig. 21 Comparisons between simulation and test for S1

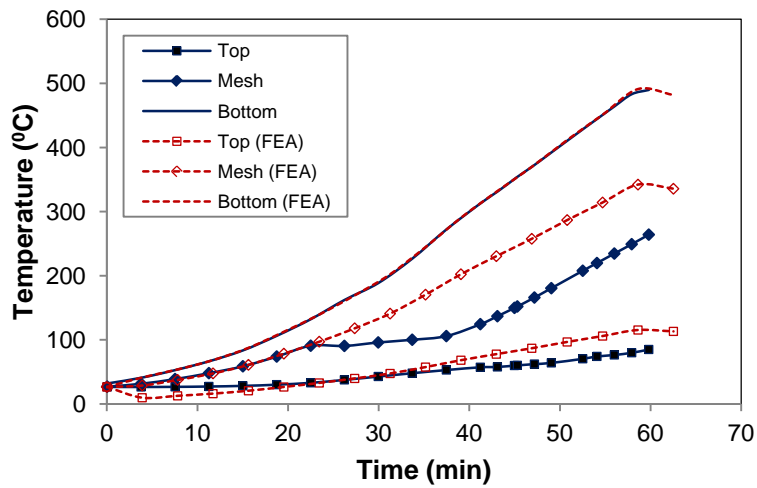


a) Temperature distribution of slab

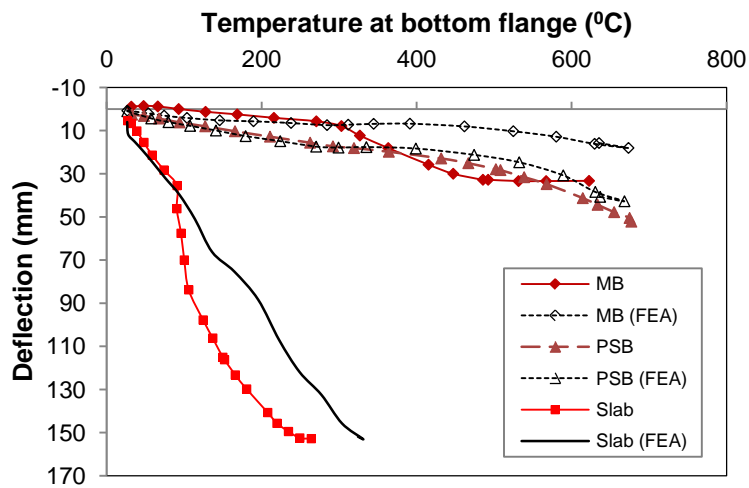


b) Deflection comparison

Fig. 22 Comparisons between simulation and test for S2-FR-IB

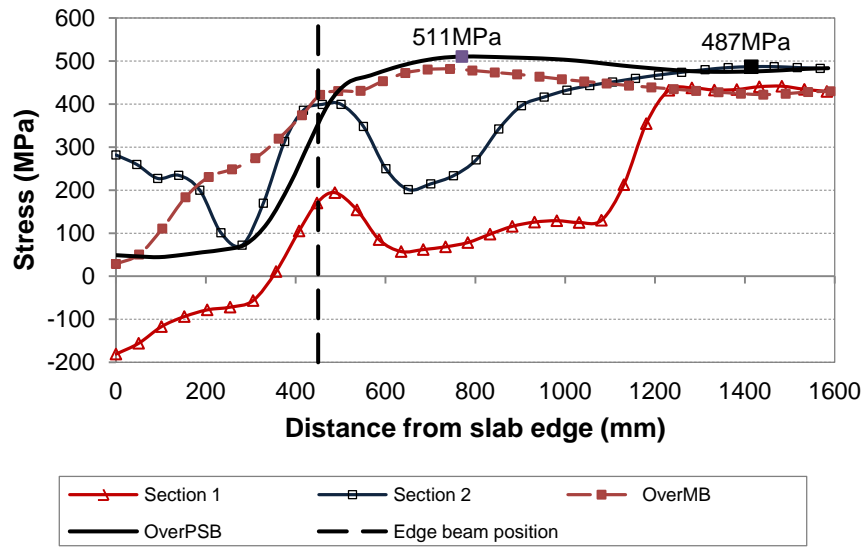


a) Temperature distribution of slab

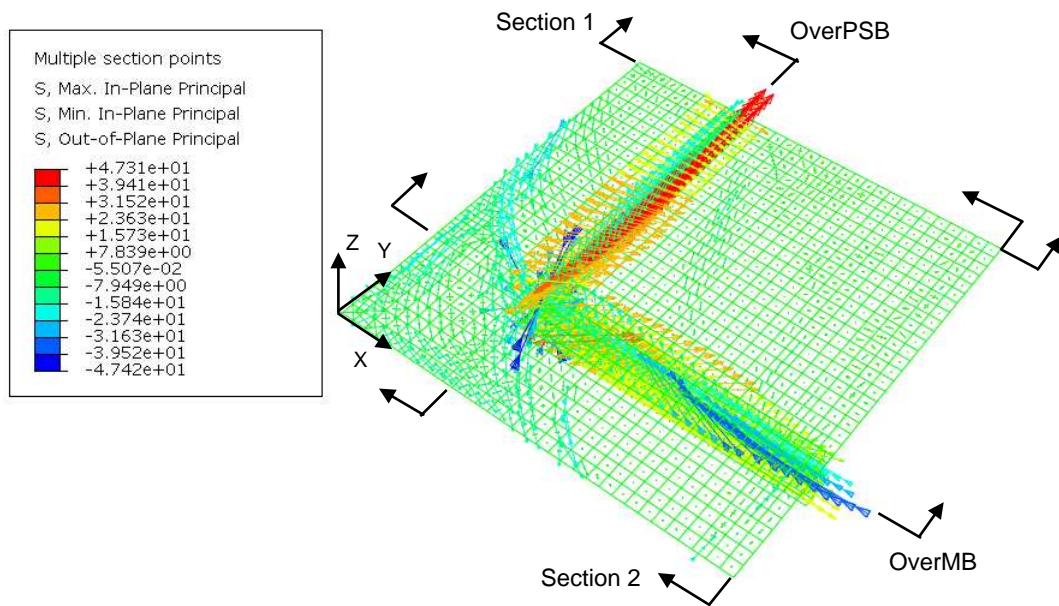


b) Deflection comparison

Fig. 23 Comparisons between simulation and test for S3-FR

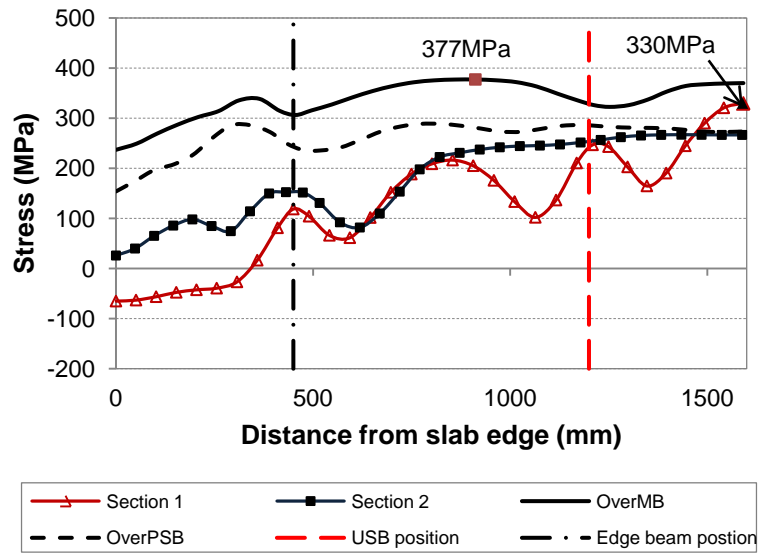


a) Stress distributions in reinforcement across the sections

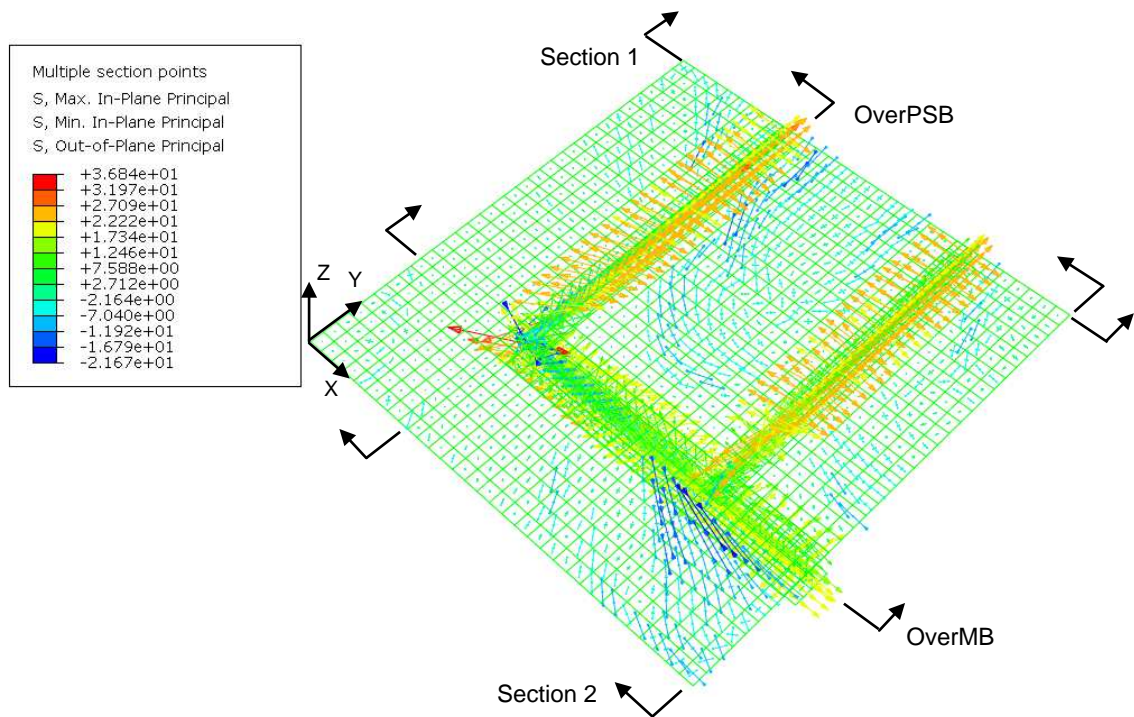


b) Principal stress distribution in concrete top surface of the slab and in the beams

Fig. 24 Numerical results of S1 at failure – 85.8 min

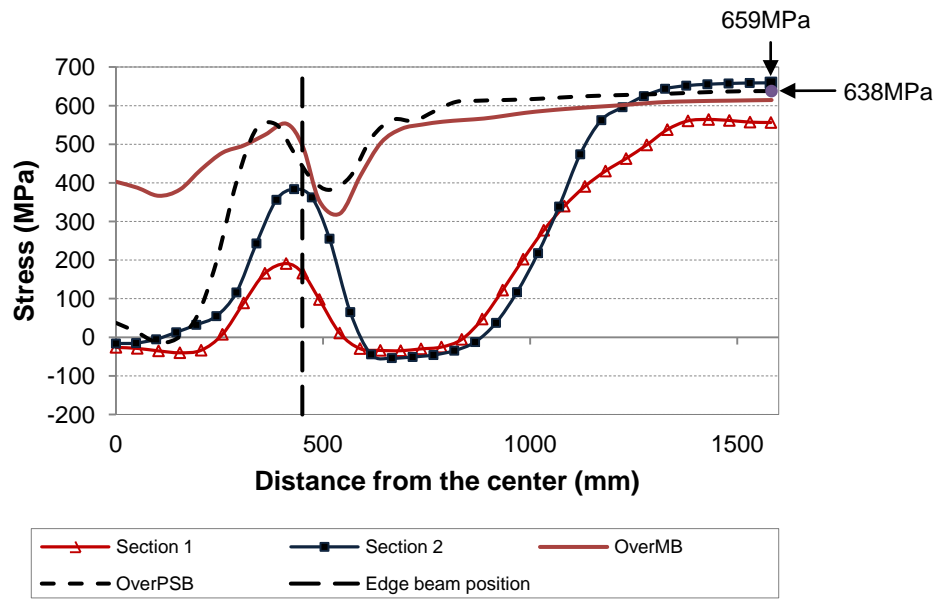


a) Stress distributions in reinforcement across the sections

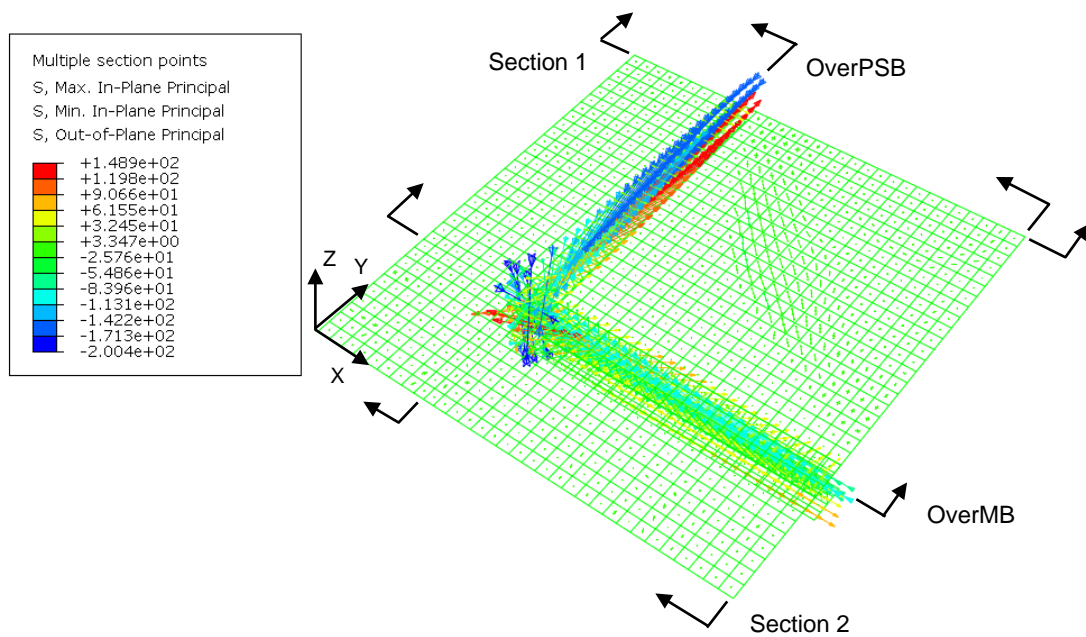


b) Principal stress distribution in concrete top surface of the slab and in the beams

Fig. 25 Numerical results of S2-FR-IB at failure – 84.0 min



a) Stress distributions in reinforcement across the sections



b) Principal stress distribution in concrete top surface of the slab and in the beams

Fig. 26 Numerical results of S3-FR at failure – 45.0 min